JACS
JOURNAL OF THE AMERICAN CHEMICAL SOCIETY

ARTICLE

pubs.acs.org/JACS

Disruption of Supported Lipid Bilayers by Semihydrophobic Nanoparticles

Benxin Jing and Yingxi Zhu*

Department of Chemical and Biomolecular Engineering, University of Notre Dame, Notre Dame, Indiana 46556, United States

Supporting Information

ABSTRACT: Understanding the interaction between functional nanoparticles and cell membranes is critical to use nanomaterials for broad biomedical applications with minimal cytotoxicity. In this work, we have investigated the effect of adsorbed *semihydrophobic* nanoparticles (NPs) on the dynamics and morphology of model cell membranes. We have systematically varied the degree of surface hydrophobicity of carboxyl end-functionalized polystyrene NPs of varied size in buffer solutions with varied ionic strength. It is observed that semihydrophobic NPs can readily adsorb on neutral SLBs and drag lipids from SLBs to NP surfaces. Above a critical NP concentration, the disruption of SLBs is observed, accompanied with the formation and rapid growth of lipid-poor regions on NP-adsorbed SLBs. In the study of the effect of solution ionic strength on NP surface hydrophobic degree and the growth of lipid-poor regions, we have concluded that the hydrophobic interaction enhanced by screened electrostatic interaction underlies the envelopment of NPs by lipids that are attracted from SLBs to the surface of NPs or their aggregates. Hence, the formation and growth of lipid-poor regions, or vaguely referred as "pores" or "holes" in the literature, can be controlled by NP concentration, size, and surface hydrophobicity, which is critical to design functional nanomaterials for effective nanomedicine while minimizing possible cytotoxicity.

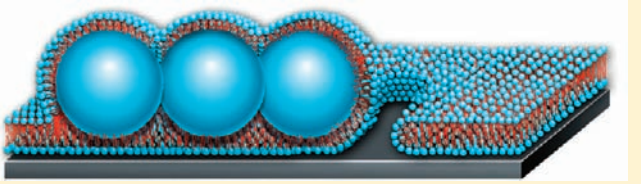

INTRODUCTION

With the blossom of nanotechnology and novel functional nanomaterials, the use of a great variety of nanomaterials has increased incredibly fast and broadly.[1] With increased application of using nanocolloids in medicine and medical diagnostics, there has been emerging interest in understanding the interaction between functional nanocolloids and cell membranes for potential application as drug delivery carriers and therapeutic agents. Conversely, the concern of nanocolloidal cytotoxicity has increased drastically in the past several years.[2−4] For example, as nanoparticles can be easily engulfed by living cells due to their small size and high surface-area-to-volume ratio, the transport of some nanoparticles (NPs) across skins and blood−brain barrier[3] has raised red flags in nanomedicine research. Although the permeability of NPs is exploited for medical diagnosis and drug delivery, exposure of cells to some biofunctional NPs might be fatal if NPs are toxic.[3] Furthermore, it has been reported that the cytotoxicity of NPs strongly depends on physicochemical properties of NPs, such as particle size and polydispersity, chemical composition, surface area, surface chemistry, and porosity.[3,5] Apparently, the current research on the interactions between NPs and cell membranes to address both benign and harmful impacts of NPs is far from enough.

Understanding the interaction between NPs and model cell membrane, i.e., lipid bilayer, can give insight into the potential biomedical application and cytotoxicity of NPs with living cells. Most recent work has thereby examined the interaction of NPs with lipid bilayers and the consequence of adsorbed NPs on the structural reconstruction and phase transition of lipid bilayers.[6−35] Structurally, a lipid bilayer consists of two monolayers of closely packed lipid molecules with their lipophilic tails shielded by their head groups from bulk aqueous solutions; thus, a lipid bilayer commonly contains both hydrophobic and hydrophilic regions, both of which could accommodate the interaction with NPs of varied surface chemistry.[36] In recent theoretical and computer simulation studies, it is found that the morphological reorganization and evolution of disrupted lipid bilayers, due to their interaction with NPs, strongly depend on the surface hydrophilicity of NPs.[32] If the hydrophilicity of NPs is sufficiently high, NPs can rapidly remove lipid molecules from lipid bilayers, resulting in an irreversible formation of "pores' or "holes" in lipid bilayers.[18,34,35] In contrast, it is predicted that no pore formation occurs with hydrophobic or Janus NPs, even though such NPs can be embedded in lipid bilayers.[23,26]

However, as no clear definition is given to explicitly describe the hydrophilic or hydrophobic degree of NPs, it remains unknown how and to what extent the disrupted structures of lipid bilayers as well as the resulting NP-induced pore formation depends on NP surface hydrophobicity. In this work, we have focused on *semihydrophobic NPs*, which can attract proteins and be used to examine the activity of antigens and antibodies, and examined their interactions with lipid bilayers at an ionic strength range similar to that in the human body; specifically we have systematically varied the fraction of surface hydrophobicity of

Received: May 2, 2011
Published: June 01, 2011

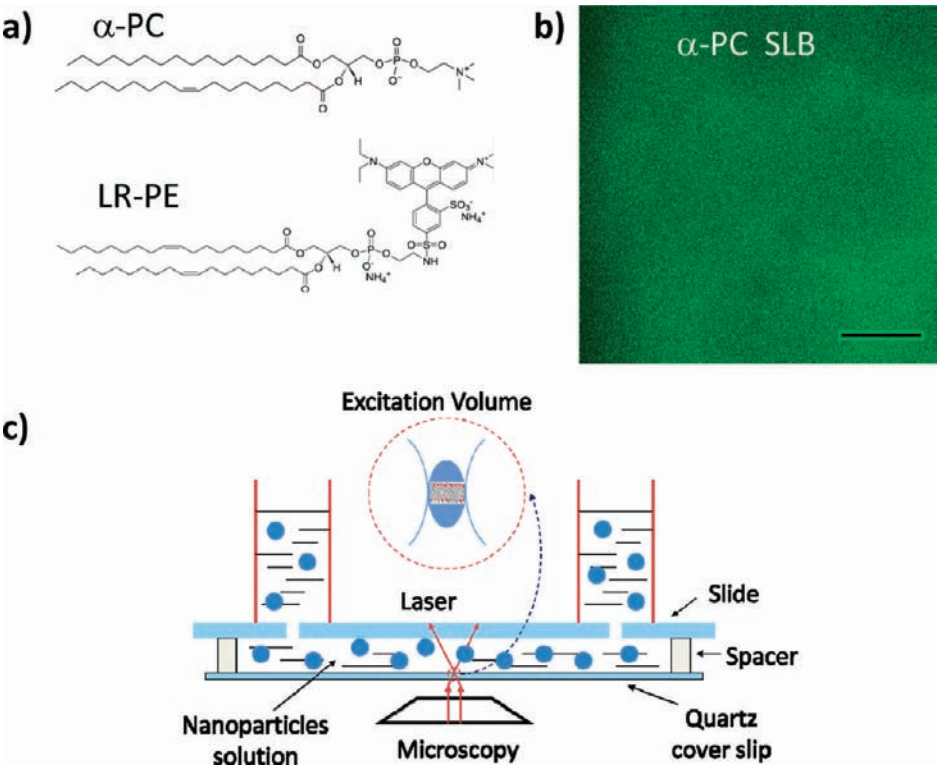

Figure 1. (a) Chemical structure of plain α-PC lipid and fluorescent LR-PE lipid probe used in this work. (b) Fluorescence micrograph confirms a homogeneous and uniform morphology of mixed SLB of α-PC and LR-PE at a molar ratio of 100:1 in the absence of cPS-NPs in PBS buffer solution. The scale bar in the fluorescence micrograph is 20 μm. (c) Schematic of experimental setup.

ionizable end-functionalized NPs of varied size and directly examined its effect on the morphological evolution of supported neutral lipid bilayers via direct microscopic and spectroscopic observation. We have observed that adsorbed semihydrophobic NPs can deform supported lipid layers (SLBs) and also readily remove lipids from SLBs to envelop adsorbed NPs and produce lipid-poor regions or apparent microscaled pores. To further investigate the driving force responsible for the envelopment of NPs by dragged lipids, we have also varied the medium ionic strength to explore the possible contribution of hydrophobic and electric static interaction to the formation of NP−lipid complexes.

EXPERIMENTAL DETAILS

Materials. L-α-Phosphatidylcholine (α-PC) and fluorescent 1,2-dioleoyl-*sn*-glycero-3-phosphoethanolamine-*N*-(lissamine rhodamine B sulfonyl) ammonium (LR-PE), both purchased from Avanti Polar Lipids, are used as supported lipid bilayers (SLBs) on quartz coverslip (ESCO products). The chemical structure of both α-PC and LR-PE is shown in Figure 1a. Phosphate-buffered saline (PBS) buffer solutions (VWR) are used to simulate the ionic environment in the human body. They are also diluted with varied amounts of deionized water (Barnstead Nanopure II) to vary medium ionic strength.

Carboxyl-end-functionalized polystyrene nanoparticles (cPS-NPs) of varied diameter, d = 28, 62, and 140 nm, are purchased from Invitrogen, whose surface charge density, σ, in deionized water is reported as 0.017, 0.047, and 0.162 charge/nm^2 by Invitrogen. The σ of 140 nm cPS-NPs in PBS buffer with different ionic strength is determined by the measurement of nanoparticle zeta potential, ζ (Brookhaven Instruments, ZetaPlus), according to the following equation,[37,38]

$$\sigma = \frac{4\pi a^2 \varepsilon_r \varepsilon_0 k_B T}{e^2 \lambda_D}\left[exp\left(\frac{e\zeta}{2k_B T}\right) - exp\left(-\frac{e\zeta}{2k_B T}\right) + \frac{4\lambda_D}{a}\cdot\frac{exp\left(\frac{e\zeta}{2k_B T}\right) - 1}{exp\left(\frac{e\zeta}{2k_B T}\right) + 1}\right] \quad (1)$$

where ε_r (≈78) is the dielectric constant of water, λ_D is the Debye screening length, and a is the radius of cPS-NPs. From measured σ, the surface density of carboxyl functional groups is estimated to range from 0.01 to 0.16 carboxyl end functional group/nm^2, which is at least 1 order of magnitude lower than that of surface-grafted poly-(carboxylic acid) layer on PS-NPs that are regarded as hydrophilic NPs. Unlike those hydrophilic PS-NPs whose surface is grafted with hydrophilic polymers with a great many ionizable groups, the surface of cPS-NPs used here is hydrophobic polystyrene surface with sparse ionizable groups; thus, we loosely define cPS-NPs used in this work as semihydrophobic NPs. To quantify the semihydrophobic degree of cPS-NPs, we have tentatively estimated the fraction of hydrophobic patches, FHP, on cPS-NPs in varied PBS buffers as

$$\mathrm{FHP} = 1 - \pi\lambda_D^2/(e/\sigma) \quad (2)$$

where $\pi\lambda_D^2$ is the area of each charged surface patch on a cPS-NP in varied salt solutions based on the Debye−Hückel theory, e/σ is the area of each charged surface patch on a cPS-NP in deionized water, and the obtained FHP results of cPS-NPs of d = 140 nm at varied PBS concentrations are summarized in Table 1.

Semihydrophobic cPS-NPs are well dispersed in PBS buffer solutions of varied PBS volume fraction. Double-side polished quartz coverslips are used as the solid substrate and cleaned by first sonication in ethanol for 10 min followed by soaking in a heated piranha solution (30% H_2O_2

Table 1. Measured Zeta Potential, ζ, Estimated Surface Charge Density, σ, and Fraction of Hydrophobic Patches, FHP, of cPS-NPs of d = 140 nm Suspended in Buffer Solutions of Varied PBS Volume Fraction That Leads to the Variance in Measured Medium Conductivity as Well as Estimated Debye Screening Length, λ_D

PBS fraction in aqueous solutions	0.2 × PBS	0.4 × PBS	0.6 × PBS	0.8 × PBS	1 × PBS
medium conductivity (S/m)	0.73	1.37	1.97	2.52	3.33
λ_D (nm)	1.64	1.16	0.95	0.82	0.74
measured ζ (mV)	−54.94 ± 2.84	−42.92 ± 4.52	−37.24 ± 2.32	−34.86 ± 1.48	−29.48 ± 3.82
σ (charge/nm^2) [a]	0.033	0.024	0.021	0.019	0.016
FHP[b]	0.72	0.90	0.94	0.96	0.97

[a] The surface charge density, σ, is estimated based on measured zeta potential, ζ, of cPS-NP of d = 140 nm in varied PBS buffer solution by using eq 1. [b] The fraction of hydrophobic patches, FHP, on cPS-NPs in PBS buffer is estimated based on the determined σ of cPS-NPs in PBS solutions of varied λ_D by using eq 2 simply based on the double-layer electrostatic screening picture.

and 70% H_2SO_4) at temperature T = 120 °C for 2 h. Subsequently, quartz surfaces are thoroughly rinsed with deionized water and dried with nitrogen gas (purity >99.9%) before use.

Preparation of Supported Lipid Bilayers (SLBs). α-PC SLBs are prepared by rupturing and spreading small unilamellar vesicles (SUVs) on a quartz coverslip. SUVs are prepared by the commonly used extrusion method:[39] Briefly, a mixture of 250 μL of 20 mg/mL α-PC solution with 86 μL of 1 mg/mL LR-PE in chloroform is dried by nitrogen gas to form a dry mixed lipid film and then resuspended in 1.2 mL of PBS buffer to form lipid vesicles via sonication over 20 min first and again after storage at T = −25 °C overnight. Subsequently, the suspension of hydrated lipid vesicles is extruded repeatedly through a miniextruder (Avanti Polar Lipids) with two layers of polycarbonate membrane filters of 100 nm pore diameter (Whatman, Maidstone, UK) to yield SUVs of mixed α-PC and LR-PE of d = 134 ± 11 nm as determined by dynamic light scattering (Brookhaven Instruments). For all the fluorescence microscopic in this work, the ratio of plain α-PC to fluorescent LR-PE in the mixed SLBs is kept constant at 100:1 for fluorescence microscopic experiments but 10^5:1 for single-molecule spectroscopic experiments.

One milliliter of SUV solution in PBS buffer solution is added to a cleaned quartz coverslip and kept incubated in a custom-built liquid cell as shown in Figure 1c for 45 min to obtain a supported lipid bilayer. Excess SUVs are removed by repeatedly and gently rinsing the SLB with PBS buffer first followed with deionized water. Finally, SUV-free supported lipid bilayers are suspended in aqueous solutions of varied PBS fraction before experiments. The homogeneity of fluorescent lipid bilayer is examined by confocal laser scanning microscopy as exhibited in Figure 1b.

Characterization. The adsorption of cPS-NPs on the SLB of mixed α-PC and LR-PE at a molar ratio of 100:1 is quantified by quartz crystal microbalance (QCM) with a fluid cell (Stanford Research System, QCM200). The morphology of α-PC and LR-PE mixed SLBs with and without cPS-NPs is characterized at real time by confocal laser scanning microscopy (CLSM) (Zeiss LSM 5 Pascal) with a 100× objective lens (NA = 1.4, oil immersion) and analyzed by ImageJ.[40]

The dynamics of fluorescent LR-PE probe in the mixed SLBs upon the adsorption of cPS-NPs of varied size in aqueous solutions of varied PBS concentration is characterized at a single-molecule resolution by fluorescence correlation spectroscopy (FCS), which is set up on an inverted microscope (Zeiss Axio A1) equipped with a 100× objective lens (NA = 1.4, oil immersion), as detailed elsewhere.[41,42] Briefly, an argon laser (Melles Griot, λ_{ex} = 488 nm) is focused on the SLB aqueous interface by reaching maximum fluorescence photon count detected by two single-photon-counting modules (Hamamatsu), which is also confirmed by a CCD camera (Andor iXon) with the smallest optical diffraction spot at the surface. The emission fluorescence intensity, $I(t)$ of fluorescent LR-PE lipid, in the mixture with plain α-PC lipids, over a small focal volume, which is calibrated as ω_{xy} = 250 nm in the lateral diameter and ω_z = 7.3 μm in the vertical height by using Alexa Flour 488 (Invitrogen) of known diffusion coefficient in a dilute bulk solution, is measured to obtain the autocorrelation function

$$G(\tau) = \langle \delta I(t)\delta I(t+\tau)\rangle / (\langle I(t)\rangle)^2 \quad (3)$$

The surface diffusion coefficient, D, as well as the surface concentration, $[c]$, of fluorescent LR-PE probe in α-PC SLBs is thus determined from $G(\tau)$ by fitting it with the two-dimensional Gaussian equation

$$G(\tau) = (\pi\omega_{xy}^2[c])^{-1}(1 + (4D\tau)/(\omega_{xy}^2))^{-1} \quad (4)$$

Both FCS and CLSM measurements are conducted with a liquid cell as shown in Figure 1c.

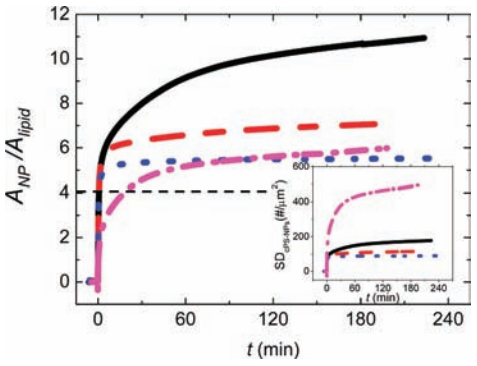

Figure 2. Time-dependent adsorption of 3.3 nM cPS-NPs of d = 62 nm in 1 × PBS solution (pink dot-dash line), 140 nm in 1 × PBS (black solid line), 0.6 × PBS (red dash line), and 0.2 × PBS solution (blue dot line) on α-PC and LR-PE mixed SLBs as described by the ratio of total surface area of absorbed cPS-NPs, A_{NP}, to total surface area of α-PC SLB, A_{lipid}. Inset: Surface density, SD (unit: NP number per SLB area, #/μm^2) of absorbed cPS-NPs on α-PC SLB against elapsed time.

RESULTS AND DISCUSSIONS

Semihydrophobic cPS-NPs are found to readily adsorb on α-PC SLBs from PBS aqueous suspensions as characterized by QCM. Over a short time period less than 2 min, an adsorption equilibrium from PBS solutions on α-PC SLBs is achieved with cPS-NPs of d = 62 and 140 nm as shown in Figure 2, yet the mass of adsorbed NPs of d = 28 nm is probably too small to be detected by QCM. Based on the estimated surface density of cPS-NPs on α-PC SLBs as shown in the inset of Figure 2, we can describe the adsorbed amount of NPs on SLBs in term of total

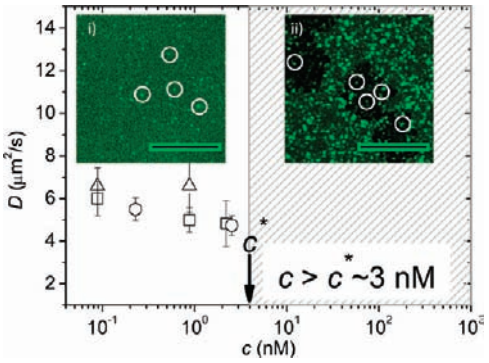

Figure 3. Measured diffusion coefficient, D, of single LR-PE lipid probes in mixed α-PC and LR-PE SLBs against the concentration, c, of cPS-NPs of d = 28 nm (squares), 62 nm (circles), and 140 nm (triangles) in 1 × PBS solutions. Inset: Fluorescence micrographs show the morphology of mixed α-PC and LR-PE SLBs with adsorbed cPS-NPs in 1 × PBS solution at (i) c = 0.8 nM (below c*) and (ii) c = 8.2 nM (above c*). The scale bar for both images is 10 μm. White circles indicate fluorescent bright microdomains in the "dark" lipid-poor regions, suggesting the adsorption of lipids on the surface of cPS-NPs.

surface area of NPs, A_{NP}, per α-PC lipid bilayer area, A_{lipid}. It needs to be noted that the ratio of A_{NP}/A_{lipid} = 4 suggests a full coverage of a cPS-NP monolayer on the surface of α-PC SLBs, while A_{NP}/A_{lipid} > 4 suggests a possible multilayer of cPS-NPs or their aggregates on α-PC SLBs. The amount of adsorbed cPS-NPs increases with increasing the PBS concentration in the buffer solutions, showing a strong dependence of ionic strength, which suggests the facilitation of cPS-NP adsorption on α-PC SLBs by screening electrostatic interaction.

To investigate the effect of adsorbed cPS-NPs on the structural reorganization of α-PC SLBs, we first examine the dynamics of single LR-PE lipids in fluid α-PC SLB at T = 25 °C with increased NP concentration. As shown in Figure 3, with low NP concentration in PBS buffer solutions, the measured D of LR-PE remains nearly unchanged upon NP adsorption or shows a negligibly small decrease possibly due to the NP-adsorption-induced "slaved diffusion".[43] However, when the NP concentration exceeds a critical value, $c^* \sim 3$ nM, the D of LR-PE becomes immeasurable by FCS, indicating a significant suppression of lipid mobility in α-PC SLB. According to the amount of absorbed NPs measured by QCM, the coverage of NPs on α-PC SLBs has reached the saturation at $c^* \sim 3$ nM. It should be pointed out that despite a drastic reduction of lipid dynamics due to cPS-NP adsorption, α-PC SLB with adsorbed NPs remains in the fluid phase as evidently supported by the observation of rapid fluorescence recovery of LR-PE lipids in the photobleached regions in the mixed SLB using a high-intensity laser of 100 mW (see Supporting Information Figure S1). The critical NP concentration of $c^* \sim 3$ nM is confirmed to be the same with cPS-NPs of varied d = 28−140 nm, indicating its independence of NP size. At cPS-NP concentration, $c < c^*$, the morphology of α-PC SLBs appears homogeneous and uniformly fluorescent with the presence of some bright fluorescent microdomains of varied size in the range of 0.3−0.6 μm as circled in Figure 3i, which suggests the possible adsorption of lipid molecules onto the surface of cPS-NPs. In sharp contrast, at $c > c^* \sim$ 3nM, an apparent pore formation on α-PC SLBs with adsorbed cPS-NPs of d = 62 nm is observed as fluorescence micrographs are exhibited in Figure 3ii. According to previous theoretical and computer simulation predictions with tense lipid bilayers, the critical NP concentration is related to the threshold tension imposed on lipid bilayer; with increased NP adsorption at $c \geq c^*$ where a partial envelopment of a NP with lipid molecules can be achieved, the threshold tension on the SLB is exceeded to cause the stretching and instability of α-PC SLB, thereby initiating the pore formation.

It should be noted that in our microscopic study of the morphological evolution of α-PC and LR-PE mixed SLB, the observed dark "pore" areas actually indicate the *lipid-poor* regions, while the fluorescent areas correspond to the *lipid-rich* regions. In addition, it is very intriguing to observe a sparse distribution of bright fluorescent microdomains of typically 0.3−1 μm in size as circled in the lipid-poor regions, suggesting the presence of lipid-adsorbed cPS-NPs or their aggregates in the lipid-depleted regions. Nevertheless, we expect that NP-induced pores are formed on tensed SLBs, while the size of actual pores, as reported by AFM and other experimental studies[34,35] as well as computer simulation predictions,[17,24,25,33] is possibly in the nanometer range with a dependence of NP size and surface hydrophobicity, which is much smaller than that of our observed microscaled lipid-poor regions so as not to be observed by CLSM. Hereafter we generally designate the fluorescent dark areas as lipid-poor regions in this work.

To further understand the NP-induced formation of lipid-poor regions on SLBs, we have examined the effect of NP size on the morphology of α-PC SLBs in situ by CLSM. With cPS-NP of d = 28 and 140 nm at $c > c^* \sim$ 3 nM, similar lipid-poor regions appear and grow on α-PC SLBs in PBS buffer solutions as fluorescence micrographs are shown in Figure 4a and 4b, respectively. Furthermore, as spatial distribution of fluorescence intensity on α-PC SLBs is examined by both CLSM and FCS (data are not shown), it is intriguing to find out that fluorescence intensity in the lipid-rich regions always decreases to a significantly low level after adding NPs while fluorescence intensity in the lipid-poor regions sometimes increases over time, the latter of which is supported by the observed presence of bright fluorescent microdomains associated with lipid-adsorbed NPs or aggregates with cPS-NPs of d = 62 nm (see Figure 3ii) and 140 nm (see Figure 5a-iv and b-iv), but not with cPS-NPs of d = 28 nm. The presence of fluorescent microdomains in the lipid-poor regions suggests that lipids can be dragged from α-PC SLBs to the surface of cPS-NPs or their aggregates, which agrees with recent computer simulation prediction with NP-induced pores formation on SLBs.[17,32,34] More interestingly, with cPS-NPs of d = 140 nm, we have observed the apparent "fluorescence inversion" as exhibited in Figure 4b, where the originally lipid-poor regions appear to become gradually brightened with time, suggesting a significant amount of lipid molecules transferring from lipid-rich regions onto cPS-NPs. Although A_{NP} is about fourfold A_{lipid} upon the saturation of NP adsorption on SLBs according to the QCM data shown in Figure 2, it is estimated that ~50% surface coverage of NPs, corresponding to the upper half of NP surface area exposed to the suspension, could initially accommodate the lipids that are dragged from SLBs to form a lipid monolayer; over time, as more α-PC and LR-PE lipids are dragged from SLBs to adsorb on the surface of cPS-NPs or their aggregates to form NP-cored lipid micelles, thereby showing "fluorescence inversion", as illustrated in Figure 4b-v. As such, we expect that the lipid-poor regions could be comprised of the actual holes in the stretched SLB as well as cPS-NPs enveloped with a low amount of transferred lipids from SLB. With cPS-NP

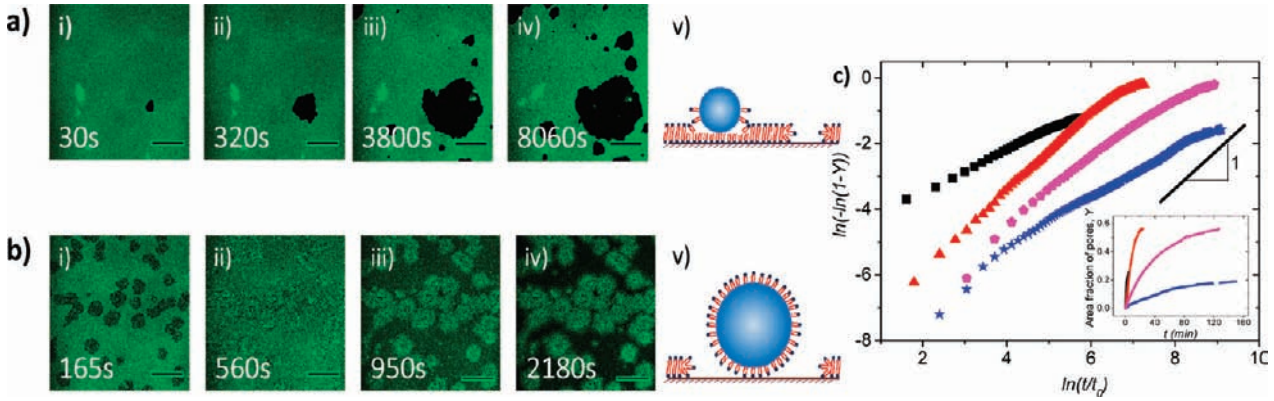

Figure 4. (Panels i–iv) Fluorescence micrographs show the morphological evolution of mixed α-PC and LR-PE SLBs after adding cPS-NPs of (a) d = 28 nm and (b) d = 140 nm, both at c = 3.3 nM in 1 × PBS solutions, against varied elapsed time as labeled in each panel. Panels v in both (a) and (b) are the schematic illustration of the morphology of lipid bilayers upon the adsorption of cPS-NPs of d = 28 and 140 nm in 1 × PBS solutions, respectively. The scale bars in all the fluorescence images are 20 μm. (c) Fraction, Y, of the area of lipid-poor regions to that of the entire SLB is determined against elapsed time to characterize the growth of lipid-poor regions due to the adsorption of cPS-NPs of d = 140 nm (squares), 62 nm (triangles), and 28 nm (stars) at c = 3.3 nM as well as the adsorption of cPS-NPs of d = 28 nm at c = 6.6 nM (pentagons). The slope of the logarithmic plot of $-\ln(1 - Y)$ against normalized time, t, by unit time, t_o = 1 s, at longer time after an initial stage approximates to 1, suggesting the applicability of the JMAK model to describe the growth of lipid-poor region via a nucleation and growth process. Inset: plot of Y against t with the same symbols as denoted in the main panel of (c).

of d = 28 nm whose size is comparable to the thickness of SLBs, cPS-NPs can be embedded and enveloped within a locally deformed SLB with much energy penalty to stretch and deform SLBs[22] as illustrated in Figure 4a-v. It is also the possible reason that there are no visible bright microdomains on the surface of cPS-NPs of d = 28 nm.

Once lipid molecules are depleted from SLBs, these lipid-poor regions appear to expand rapidly over time. As summarized in Figure 4c, we have examined the kinetics of the space-spanning of lipid-poor regions on SLBs, which is considered critical to control the size and distribution of NP-induced pores toward the applications of drug delivery and gene therapy as well as minimizing cytotoxicity.[11] As shown in the inset of Figure 4c, the growth of lipid-poor regions against elapsed time exhibits an "S" shape, suggesting a typical heterogeneous nucleation and growth process. We have tentatively applied the Johnson–Mehl–Avrami–Kolmogorov (JMAK) theory,[44–46] a widely adopted theory to describe nucleation and growth processes that occur randomly over an entire untransformed area of a given system, to examine the increase of the fraction, Y, of total lipid-poor areas over the entire SLB area against elapsed time, t. As evidently shown in Figure 4c, the logarithmic plot of measured $-\ln(1 - Y)$ against normalized t by unit time, t_o (=1 s), can be fitted linearly, in good agreement with the JMAK theoretical prediction of

$$Y = 1 - \exp(Kt^n) \qquad (5)$$

where K and n are both fitting parameters related to the detailed mechanisms of transport, nucleation, and growth. The slope, n, of the plots over longer time after the initial stage approaches 1 with all varied d, thereby showing the NP-size independence of the growth of lipid-poor regions; in addition, it is observed in Figure 4c that the lipid-poor regions grow faster with larger cPS-NPs at higher NP concentration; as combined, it is suggested that such a kinetics of the two-dimensional growth the lipid-poor regions is possibly controlled by the diffusion of lipid molecules, further supporting the applicability of the JMAK model to describe the NP-induced morphological disruption of SLBs.[47]

Accordingly, all the above observations lead to a central key question: what is the driving force to drag lipid molecules from a SLB to a cPS-NP surface? With zwitterionic polar head of both α-PC and LR-PE lipids, it is theoretically predicted that both positively and negatively charged NPs can induce pores on SLBs;[32] furthermore, the higher the NP surface charge density, the easier for the pore formation as predicted. In our case, we originally speculate that the electrostatic attraction between carboxyl terminal groups on cPS-NPs and lipid polar heads could be favored with highly charged NPs because the outside group of lipid polar head is slightly positively charged when facing the bulk aqueous solution. To further examine this scenario, we have systematically varied ionic strength in the suspensions of cPS-NPs of d = 140 nm. Based on measured ζ, we have estimated the σ, by using eq 1, and FPH of cPS-NPs, by using eq 2 , which is derived from a rough model considering the electrostatic screening effect. As summarized in Table 1, both surface charge density, σ, and hydrophilic degree, in terms of 1 − FHP, of cPS-NPs of d = 140 nm increase with decreasing solution ionic strength by diluting 1 × PBS buffer solutions. However, as shown in Figure 2, the adsorption of cPS-NPs is much weakened by decreasing solution ionic strength, suggesting that another kind of NP–lipid interaction underlies the adsorption of cPS-NPs as well as the induced disruption of SLBs. Subsequently, we examine the morphological evolution of α-PC and LR-PE mixed SLBs with adsorption of cPS-NPs of d = 140 nm in PBS buffer solutions of varied ionic strength. Apparently, as shown in Figure 5, the growth of lipid-poor regions is considerably suppressed with decreased ionic strength, whose trend is clearly opposite to the theoretical prediction[32] that increasing the surface charge density of hydrophilic NPs leads to enhancing the pore formation. It should be also noted that no aggregation is observed with cPS-NPs of d = 140 nm in all varied PBS buffer solutions by dynamic light scattering, which thus excludes the responsibility of adsorbed NP aggregates for the growth of lipid-poor regions. As such, based on the observations of increased NP adsorption and

dx.doi.org/10.1021/ja2040305 |J. Am. Chem. Soc. 2011, 133, 10983–10989

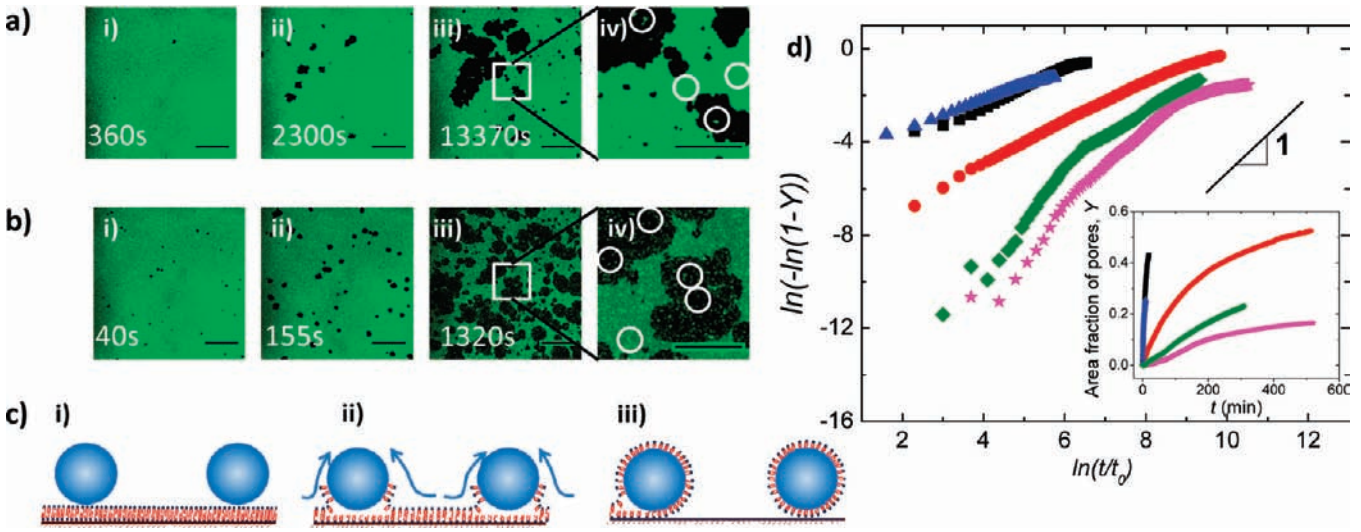

Figure 5. Fluorescence micrographs in panels i—iii show the morphological evolution of mixed α-PC and LR-PE SLBs after adding cPS-NPs of d = 140 nm in (a) 0.2 × PBS and (b) 0.6 × PBS buffer solutions. The fluorescent bright domains that suggest lipid-enveloped cPS-NPs are indicated by white circles as shown in panels iv that is the blowout of the square area in panels iii. All the scale bars are 20 μm in panels i—iii and 10 μm in panels iv. (c) Schematic of the morphological evolution of SLBs upon the adsorption of cPS-NPs of d = 140 nm in PBS solutions suggests a process from the partial to full envelopment of cPS-NPs by attracting more lipids from SLBs, resulting in the eventual formation of NP-cored lipid micelle as observed by "fluorescence inversion". (d) Fraction, Y, of the area of lipid-poor regions to that of entire SLB as determined against elapsed time to characterize the growth of lipid-poor regions due to the adsorption of cPS-NPs of d = 140 nm at c = 3.3 nM in buffer solutions of varied PBS volume fraction, 1× (triangles), 0.8× (squares), 0.6× (circles), 0.4× (diamonds), and 0.2× (stars). The slope of the logarithmic plot of $-\ln(1 - Y)$ again normalized time, t, by unit time, t_o = 1 s, at longer time after an initial stage approximates to 1. Inset: Plot of Y against t with the same symbols as denoted in the main panel of (d).

enhanced formation and growth of NP-induced lipid-poor regions with increased NP hydrophobicity, we derive that the hydrophobic interaction is the dominant driving force to drag lipid molecules from SLB to adsorb and wrap on cPS-NPs, which can be further facilitated by the electric screening effect at increased ionic strength; thus, the hydrophobic interaction as the driving force with semihydrophobic NPs is clearly distinct from the attraction between lipid polar heads and charged surface patches of hydrophilic NPs as the driving force as predicted in the literature.[32] With increasing ionic strength to screen electrostatic interaction between NPs and lipid head groups, the surface hydrophobicity of cPS-NPs apparently increases, indicating more hydrophobic patches to attract and accommodate lipid molecules from SLBs. Therefore, we expect that a monolayer of lipid molecules with lipophilic tails interacting with NP hydrophobic surface could be formed with cPS-NPs;[22] with increased adsorption and insertion of large cPS-NPs of d = 140 nm on SLBs to consequently attract more neighboring lipids to their colloidal surfaces, the lipid-poor regions further grow with time, which is accompanied by the increased envelopment of cPS-NP with lipid monolayers, thereby leading to the observed "fluorescence inversion" corresponding to NP-cored lipid micelles, as illustrated in Figure 5c. Consistently, the faster growth of lipid-poor regions with higher PBS concentration also supports the scenario of NP—lipid hydrophobic interaction facilitated by screened electrostatic interface to cause the envelopment of cPS-NP by lipids as quantified in Figure 5d. Additionally, the JMAK prediction is generally confirmed with buffer solutions of varied PBS concentration. Cautiously, a deviation from the linear fitting is observed in 0.2× and 0.4× PBS buffer solutions, showing a fast growth at the early stage, followed by a slow growth at further elapsed time. Yet, more rigorous models are under current exploration to better describe the NP-induced growth of lipid-poor regions in dilute PBS solutions.

CONCLUSION

In this work, we have systematically investigated the effect of semihydrophobic NPs on the interaction between NPs and SLBs and the resulting morphological reorganization of disrupted SLBs. We have observed that semihydrophobic NPs can be readily adsorbed on SLBs and drag lipids from SLBs to NP surfaces. A critical NP concentration is found to initiate the disruption of SLBs with the resulting formation of lipid-poor regions. With the investigation of the effect of solution ionic strength on NP surface hydrophobic degree and the growth of lipid-poor regions, we have concluded that the hydrophobic interaction enhanced by screened electrostatic interaction underlies the envelopment of NPs by lipids that are attracted from SLBs; furthermore, hydrophobic attraction, with screened electrostatic repulsion at high ionic strength, can largely facilitate the formation of patched lipid bilayers on large NPs to further enhance the formation and growth of lipid-poor regions on SLBs. We expect that similar behaviors can be observed with supported lipid bilayers on other hydrophilic substrates, such as mica and glass, where lipid bilayers can be initially formed, yet the degree of the NP-induced disruption of lipid bilayers and the resulting pore formation could strongly depend on the surface chemistry and roughness of substrates, which might be worth further investigation. In summary, the formation and growth of lipid-poor regions, or vaguely referred as "pores" or "holes" in the literature, can be controlled by NP concentration, size, and surface hydrophobicity, which is critical to design functional nanomaterials for effective nanomedicine while minimizing possible cytotoxicity.

■ ASSOCIATED CONTENT

Supporting Information. Supporting experimental results and figures. This material is available free of charge via the Internet at http://pubs.acs.org.

■ AUTHOR INFORMATION

Corresponding Author
yzhu3@nd.edu

■ ACKNOWLEDGMENT

We are grateful to Drs. Shengqin Wang and Jiang Zhao for help and discussion. This work is supported by the U.S. Department of Energy, Office of Basic Energy Science, Division of Materials Science and Engineering (DE-FG02-07ER46390).

■ REFERENCES

(1) http://www.nanotechproject.org/inventories/consumer/.
(2) Wick, P.; Manser, P.; Spohn, P.; Grass, R. N.; Limbach, L. K.; Bruinink, A.; Stark, W. J. *Environ. Sci. Technol.* **2006**, *40*, 4374–4381.
(3) Yang, Z.; Liu, Z. W.; Allaker, R. P.; Reip, P.; Oxford, J.; Ahmad, Z.; Ren, G. *J. R. Soc. Interface* **2010**, *7*, S411–S422.
(4) http://www.ph.ucla.edu/ehs/uctsrtpnano/.
(5) Xu, M.; Fujita, D.; Kajiwara, S.; Minowa, T.; Li, X.; Takemura, T.; Iwai, H.; Hanagata, N. *Biomaterials* **2010**, *31*, 8022–8031.
(6) Yang, K.; Ma, Y.-Q. *Nat. Nano.* **2010**, *5*, 579–583.
(7) Tomasini, M. D.; Rinaldi, C.; Tomassone, M. S. *Exp. Biol. Med.* **2010**, *235*, 181–188.
(8) Lin, X.; Li, Y.; Gu, N. *J. Comput. Theor. Nanosci.* **2010**, *7*, 269–276.
(9) Li, Y.; Gu, N. *J. Phys. Chem. B* **2010**, *114*, 2749–2754.
(10) Yan, L.-T.; Yu, X. *Macromolecules* **2009**, *42*, 6277–6283.
(11) Yan, L.-T.; Yu, X. *ACS Nano* **2009**, *3*, 2171–2176.
(12) Wallace, E. J.; Mark, S. P. S. *Nanotechnology* **2009**, *20*, 045101.
(13) Roiter, Y.; Ornatska, M.; Rammohan, A. R.; Balakrishnan, J.; Heine, D. R.; Minko, S. *Langmuir* **2009**, *25*, 6287–6299.
(14) D'Rozario, R. S. G.; Wee, C. L.; Wallace, E. J.; Sansom, M. S. P. *Nanotechnology* **2009**, *20*, 115102.
(15) Monticelli, L.; Salonen, E.; Ke, P. C.; Vattulainen, I. *Soft Matter* **2009**, *5*, 4433–4445.
(16) Lee, H.; Larson, R. *Molecules* **2009**, *14*, 423–438.
(17) Jonghyun, P.; Wei, L. *Phys. Rev. E* **2009**, *80*, 021607.
(18) Chen, J.; Hessler, J. A.; Putchakayala, K.; Panama, B. K.; Khan, D. P.; Hong, S.; Mullen, D. G.; DiMaggio, S. C.; Som, A.; Tew, G. N.; Lopatin, A. N.; Baker, J. R.; Holl, M. M. B.; Orr, B. G. *J. Phys. Chem. B* **2009**, *113*, 11179–11185.
(19) Wong-Ekkabut, J.; Baoukina, S.; Triampo, W.; Tang, I. M.; Tieleman, D. P.; Monticelli, L. *Nat. Nano.* **2008**, *3*, 363–368.
(20) Wang, B.; Zhang, L.; Bae, S. C.; Granick, S. *Proc. Natl. Acad. Sci. U.S.A.* **2008**, *105*, 18171–18175.
(21) Shi, X.; Kong, Y.; Gao, H. *Acta Mech. Sin.* **2008**, *24*, 161–169.
(22) Roiter, Y.; Ornatska, M.; Rammohan, A. R.; Balakrishnan, J.; Heine, D. R.; Minko, S. *Nano Lett.* **2008**, *8*, 941–944.
(23) Li, Y.; Chen, X.; Gu, N. *J. Phys. Chem. B* **2008**, *112*, 16647–16653.
(24) Kelly, C. V.; Leroueil, P. R.; Orr, B. G.; Banaszak Holl, M. M.; Andricioaei, I. *J. Phys. Chem. B* **2008**, *112*, 9346–9353.
(25) Kelly, C. V.; Leroueil, P. R.; Nett, E. K.; Wereszczynski, J. M.; Baker, J. R.; Orr, B. G.; Banaszak Holl, M. M.; Andricioaei, I. *J. Phys. Chem. B* **2008**, *112*, 9337–9345.
(26) Alexeev, A.; Uspal, W. E.; Balazs, A. C. *ACS Nano* **2008**, *2*, 1117–1122.
(27) Zhou, X.; Moran-Mirabal, J. M.; Craighead, H. G.; McEuen, P. L. *Nat. Nano.* **2007**, *2*, 185–190.
(28) Troutier, A.-L.; Ladavière, C. *Adv. Colloid Interface Sci.* **2007**, *133*, 1–21.
(29) Qiao, R.; Roberts, A. P.; Mount, A. S.; Klaine, S. J.; Ke, P. C. *Nano Lett.* **2007**, *7*, 614–619.
(30) Li, L.; Davande, H.; Bedrov, D.; Smith, G. D. *J. Phys. Chem. B* **2007**, *111*, 4067–4072.
(31) Leroueil, P. R.; Hong, S.; Mecke, A.; Baker, J. R.; Orr, B. G.; Banaszak Holl, M. M. *Acc. Chem. Res.* **2007**, *40*, 335–342.
(32) Ginzburg, V. V.; Balijepalli, S. *Nano Lett.* **2007**, *7*, 3716–3722.
(33) Lee, H.; Larson, R. G. *J. Phys. Chem. B* **2006**, *110*, 18204–18211.
(34) Mecke, A.; Uppuluri, S.; Sassanella, T. M.; Lee, D.-K.; Ramamoorthy, A.; Baker, J. J. R.; Orr, B. G.; Banaszak Holl, M. M. *Chem. Phys. Lipids* **2004**, *132*, 3–14.
(35) Hong, S.; Bielinska, A. U.; Mecke, A.; Keszler, B.; Beals, J. L.; Shi, X.; Balogh, L.; Orr, B. G.; Baker, J. R.; Banaszak Holl, M. M. *Bioconjugate Chem.* **2004**, *15*, 774–782.
(36) Verma, A.; Stellacci, F. *Small* **2010**, *6*, 12–21.
(37) Ohshima, H.; Healy, T. W.; White, L. R. *J. Colloid Interface Sci.* **1982**, *90*, 17–26.
(38) Ohsawa, K.; Murata, M.; Ohshima, H. *Colloid Polym. Sci.* **1986**, *264*, 1005–1009.
(39) Froude, V. E.; Zhu, Y. *J. Phys. Chem. B* **2009**, *113*, 1552–1558.
(40) http://rsbweb.nih.gov/ij/.
(41) Magde, D.; Elson, E.; Webb, W. W. *Phys. Rev. Lett.* **1972**, *29*, 705.
(42) Rigler, R.; Mets, Ü.; Widengren, J.; Kask, P. *Euro. Biophys. J.* **1993**, *22*, 169–175.
(43) Zhang, L.; Granick, S. *Proc. Natl. Acad. Sci. U.S.A.* **2005**, *102*, 9118–9121.
(44) Avrami, M. *J. Chem. Phys.* **1939**, *7*, 1103–1112.
(45) Avrami, M. *J. Chem. Phys.* **1941**, *9*, 177–184.
(46) Avrami, M. *J. Chem. Phys.* **1940**, *8*, 212–224.
(47) Ranganathan, S.; Von Heimendahl, M. *J. Mater. Sci.* **1981**, *16*, 2401–2404.